



CHALMERS
UNIVERSITY OF TECHNOLOGY

Polysulfide's impact on physical and electrochemical properties of ionic liquid electrolytes

Master's thesis in Applied Physics

FILIPPA LUNDIN

Department of Physics
CHALMERS UNIVERSITY OF TECHNOLOGY
Gothenburg, Sweden 2017

MASTER'S THESIS 2017

**Polysulfide's impact on physical and
electrochemical properties of ionic
liquid electrolytes**

FILIPPA LUNDIN



CHALMERS
UNIVERSITY OF TECHNOLOGY

Department of Physics
Division of Condensed Matter Physics
CHALMERS UNIVERSITY OF TECHNOLOGY
Gothenburg, Sweden 2017

Polysulfide's impact on physical and electrochemical properties of
ionic liquid electrolytes

FILIPPA LUNDIN

© FILIPPA LUNDIN, 2017.

Supervisor: Aleksandar Matic, Department of Physics,
Chalmers University of Technology, Gothenburg
Supervisor: Adam Best, Manufacturing, CSIRO, Melbourne.
Examiner: Aleksandar Matic, Department of Physics,
Chalmers University of Technology, Gothenburg

Master's Thesis 2017
Department of Physics
Division of Condensed Matter Physics
Chalmers University of Technology
SE-412 96 Gothenburg
Telephone +46 31 772 1000

Typeset in L^AT_EX
Gothenburg, Sweden 2017

Polysulfide's impact on physical and electrochemical properties of ionic liquid electrolytes

LUNDIN FILIPPA

Department of Physics

Chalmers University of Technology

Abstract

The Lithium-Sulfur battery is in need of a new safer electrolyte. For this, ionic liquids are considered a promising candidate. But how does the electrolyte react when polysulfides (PS) dissolves into it? This thesis investigates how an addition of PS affect phase transitions, ionic conductivity, mobility and SEI-formation of ionic liquid electrolytes. In the study the properties of 1-Propyl-1-methyl-pyrrolidinium Bis(fluorosulfonyl)imide (P13FSI) and 1-Butyl-1-methyl-pyrrolidinium Bis(trifluoromethanesulfonyl)imide (P14TFSI) with their corresponding anion lithium salt are compared with and without polysulfide additives. For these ionic liquid electrolytes the solubility of PS is low, hence the impact of the PS presence is small.

The phase transitions, investigated by DSC, were found to be unaffected upon addition of polysulfides for P13FSI based electrolytes, while the crystallisation temperature increases for P14TFSI based samples when polysulfides are present. The conductivity increases when PS are present in the P13FSI electrolyte, while for the P14TFSI electrolyte the conductivity decreases in the presence of PS. From diffusion coefficients the mobility of all electrolyte components was found to increase upon addition of PS for P13FSI. In the P14TFSI electrolyte the mobility decreases in the presence of PS in agreement with the result for the conductivity. From cycling and impedance data the solid electrolyte interphase (SEI) layer was found to form faster and found to have a lower resistance with PS than without for the P13FSI electrolyte. The presence of PS didn't affect the formation for the P14TFSI electrolyte. Based on this study the properties of the ionic liquid electrolytes does not change considerably when PS is introduced, making it a promising candidate as electrolyte for Lithium-Sulfur batteries.

Keywords: Ionic liquid, Li-S battery, Polysulfides, P13FSI, P14TFSI.

Acknowledgements

I would like to express my special thanks of gratitude to my two supervisors Adam Best and Aleksandar Matic that gave me the opportunity to go to Australia to do this project at CSIRO. It has been a truly amazing experience where I have learned so much!

Secondly I would also like to thank Yesim Gozukara and Roger Mulder for helping me performing the DSC and MNR measurements respectively. I am very grateful for the help I got from all of my colleagues at CSIRO but especially from Marzi Barghamadi and Steffen Jeschke. My time at CSIRO would not have been the same without you.

Lastly I would like to thank everyone back home that supported me from the other side of the world during this time; my family, friends and my boyfriend. Thank you. You mean the world to me.

Filippa Lundin, Gothenburg, June 2017

Contents

List of Figures	xi
List of Tables	xiii
1 Introduction	1
1.1 Aim	2
1.2 Limitations	2
2 Background	3
2.1 Batteries in general	3
2.2 Li-ion batteries	4
2.3 Li-S batteries	4
2.4 Electrolyte	6
2.4.1 Electrode-Electrolyte interface	7
2.5 Electrolytes for Li-S batteries	7
2.6 Ionic liquids	7
2.6.1 Ionic liquid as an electrolyte solvent	8
3 Theory	9
3.1 DSC	9
3.1.1 DSC data	9
3.2 Ionic conductivity	10
3.3 NMR	11
3.3.1 PFG spin-echo	11
3.4 Impedance	12
3.4.1 EIS	12
3.4.2 EIS to show SEI formation	13
3.5 Cycling of symmetrical cells	14
4 Experimental methods	15
4.1 Sample preparation	15
4.2 Phase transitions - DSC	16
4.3 Ionic conductivity	17
4.4 Diffusion coefficients	17
4.5 SEI	18
4.5.1 Symmetrical cell assembly	18
4.5.2 Impedance	18

4.5.3	Cycling	19
5	Results and discussion	21
5.1	Solubility of Polysulfides in Ionic Liquid	21
5.2	DSC	22
5.3	Ionic conductivity	24
5.4	NMR	25
5.5	Impedance	26
5.6	Cycling	27
6	Conclusion	31
	Bibliography	33
A	Appendix	I
A.1	Diffusion coefficients	I
A.2	Impedance	III
A.3	Cycling	VI

List of Figures

2.1	Block diagram of a cell powering an external load	4
2.2	Typical charge and discharge voltage profiles of a Li-S cell [1].	5
2.3	The structure of a typical inorganic salt to the left and an ionic liquid to the right.	8
3.1	DSC trace for P14TFSI showing glass transition, crystallisation and melting. The inset show a magnified image of the trace in the square.	10
3.2	Nyquist plot from an impedance experiment. The resistance of the electrolyte (R_1) and the SEI (R_2) are indicated in the figure.	13
3.3	SEI formation in a symmetrical cell	13
3.4	Equivalent electrical circuit of a symmetrical cell with an SEI	14
4.1	Molecular structures of P13FSI, P14TFSI, LiFSI and LiTFSI	15
4.2	Cell components of a symmetrical cell	18
5.1	P13FSI based samples	21
5.2	P14TFSI based samples	21
5.3	DSC-traces of P13FSI based electrolytes	22
5.4	DSC-traces of P14TFSI based electrolytes	23
5.5	DSC-traces showing the glass transition for P14TFSI based electrolytes.	23
5.6	Diffusion coefficients at 20 °C	26
5.7	Nyquist plot of impedance for P13FSI	26
5.8	Nyquist plot of impedance for P14TFSI	26
5.9	Impedance of symmetric cells with P13FSI based electrolytes as a function of cycle number	27
5.10	Impedance of symmetric cells with P14TFSI based electrolytes as a function of cycle number	27
5.11	Voltage profile for P14TFSI electrolyte. Inset is a magnification of the first two cycles.	28
5.12	Comparison of resistance measured from impedance and cycling data.	29
A.1	Diffusion coefficients at 40 °C	I
A.2	Diffusion coefficients at 60 °C	II
A.3	Diffusion coefficients at 80 °C	II
A.4	Impedance spectrum of P13FSI	III
A.5	Impedance spectrum of P13FSI 0.1 mol/kg LiFSI	III
A.6	Impedance spectrum of P13FSI 0.02 mol/kg Li ₂ S ₄	III

A.7	Impedance spectrum of P13FSI 0.02 mol/kg Li_2S_6	III
A.8	Impedance spectrum of P13FSI 0.1 mol/kg LiFSI 0.02 mol/kg Li_2S_4 .	IV
A.9	Impedance spectrum of P13FSI 0.1 mol/kg LiFSI 0.02 mol/kg Li_2S_6 .	IV
A.10	Impedance spectrum of P14TFSI	IV
A.11	Impedance spectrum of P14TFSI 0.1 mol/kg LiTFSI	IV
A.12	Impedance spectrum of P14TFSI 0.02 mol/kg Li_2S_4	IV
A.13	Impedance spectrum of P14TFSI 0.02 mol/kg Li_2S_6	IV
A.14	Impedance spectrum of P14TFSI 0.1 mol/kg LiTFSI 0.02 mol/kg Li_2S_4	V
A.15	Impedance spectrum of P14TFSI 0.1 mol/kg LiTFSI 0.02 mol/kg Li_2S_6	V
A.16	Voltage profile for a symmetrical cell with a P13FSI electrolyte	VI
A.17	Voltage profile for a symmetrical cell with a P13FSI 0.1 mol/kg LiFSI electrolyte	VI
A.18	Voltage profile for a symmetrical cell with a P13FSI 0.02 mol/kg Li_2S_4 electrolyte	VI
A.19	Voltage profile for a symmetrical cell with a P13FSI 0.02 mol/kg Li_2S_6 electrolyte	VI
A.20	Voltage profile for a symmetrical cell with a P13FSI 0.1 mol/kg LiFSI 0.02 mol/kg Li_2S_4 electrolyte	VII
A.21	Voltage profile for a symmetrical cell with a P13FSI 0.1 mol/kg LiFSI 0.02 mol/kg Li_2S_6 electrolyte	VII
A.22	Voltage profile for a symmetrical cell with a P14TFSI electrolyte . . .	VII
A.23	Voltage profile for a symmetrical cell with a P14TFSI 0.1 mol/kg LiTFSI electrolyte	VII
A.24	Voltage profile for a symmetrical cell with a P14TFSI 0.02 mol/kg Li_2S_4 electrolyte	VII
A.25	Voltage profile for a symmetrical cell with a P14TFSI 0.02 mol/kg Li_2S_6 electrolyte	VII
A.26	Voltage profile for a symmetrical cell with a P14TFSI 0.1 mol/kg LiTFSI 0.02 mol/kg Li_2S_4 electrolyte	VIII
A.27	Voltage profile for a symmetrical cell with a P14TFSI 0.1 mol/kg LiTFSI 0.02 mol/kg Li_2S_6 electrolyte	VIII

List of Tables

2.1	Specific capacity of lithium batteries	5
4.1	Compositions of the samples investigated	16
5.1	Sample compositions	21
5.2	Temperatures for thermal transitions in the P13FSI based electrolytes	23
5.3	Temperatures for thermal transitions in P14TFSI based electrolytes .	24
5.4	Ionic conductivity at 25 °C	25

1

Introduction

To overcome the climate challenge with global warming that we are facing today, society need to replace fossil energy as our primary energy source with renewable energy such as water, wind and solar power. Since renewable energy isn't always accessible, interest in energy storage has increased lately. A lot research is performed in the battery field to fill the need of energy storage. One application in need of better energy storage systems are electric vehicles, where today's electric vehicles are limited to driving distances of around 500-700 km/charge [2]. In order to compete with combustion engine driven vehicles the energy and power density of the battery needs to be improved. Other important parameters in this context is the cost and sustainability of the materials and methods.

The current technology dominating the market is the Li-ion battery with a practical specific capacity of about 150 mAh/g for the state-of-the-art batteries and a theoretical maximum specific capacity just under 300 mAh/g [3]. The batteries are constantly being developed and will unfortunately soon reach it's maximum capacity. To increase the capacity further one needs to go beyond Li-ion batteries.

One candidate to replace Li-ion battery is the lithium-sulfur battery. Its theoretical specific capacity is 1675 mAh/g [1], almost 6 times higher than the Li-ion battery. In practice, a specific capacity of 500-1350 mAh/g [4] is obtained which is 3-9 times higher than what has been achieved from Li-ion cells. Apart from the performance the lithium-sulfur cells are also more environmental friendly than Li-ion cells and due to the abundance of sulfur might also be cheaper and more sustainable. However, the Li-S battery still suffers from some technical difficulties, some of them being related to polysulfides (Li_2S_x) created during cycling of the cell. It is when these polysulfides leak out into the electrolyte that they cause problems in the cell, such as, short cycle life and low charging efficiency [1].

Effort has been put into preventing the polysulfides from dissolving into the electrolyte. However, some polysulfides always leak out into the electrolyte. What then is important to focus on is the electrolyte. One want an electrolyte that apart from fulfilling the requirements for an standard electrolyte also has low solubility for polysulfides and is unaffected by the presence of it. All this while the electrolyte must also be environmentally friendly and safe. One option for this is ionic liquid based electrolytes.

Despite ionic liquids being tried out as solvents in electrolytes for lithium-sulfur

batteries, few studies has been done on how ionic liquid electrolyte reacts when polysulfides are dissolved in the electrolyte. This thesis aims to investigate how polysulfides affect phase transitions, ionic conductivity, mobility and SEI-formation for ionic liquid electrolytes.

1.1 Aim

For long term cycling of Li-S batteries it is important to understand how the addition of polysulfides affects the properties of the electrolyte. This thesis aims to do so, by investigating physical and electrochemical properties of ionic liquid based electrolytes with and without polysulfides additives.

1.2 Limitations

The study has been limited to electrolytes formed by two types of ionic liquids as solvent and their corresponding anion lithium salt at the relatively low concentration of 0.1 mol/kg. Even though a higher salt concentration might be more realistic in an electrolyte for a battery application.

2

Background

When rechargeable Li-ion batteries entered the market in the 1990's it changed our society. They paved the way for portable devices that have today become an essential part of our lives, such as mobile phones, laptops and even hybrid/electric vehicles. Since its inception the Li-ion battery has been further developed and continues to be refined and improved. However, the energy density of the Li-ion battery is approaching its practical maximum and researchers are looking beyond Li-ion for other alternatives to fill the increasing need of energy storage. One of these alternative systems is the lithium-sulfur (Li-S) battery. It's theoretical specific capacity is expected to be 1675 Ah/kg with a theoretical energy density of 2600 Wh/kg, that is 3-5 times higher than the state of art Li-ion batteries [1]. Yet there are still some significant problems with Li-S batteries that need to be solved before the technology can enter the mass market. To understand what problems Li-S batteries are suffering from the following sections will explain the basics of batteries in general and lithium-sulfur in particular.

2.1 Batteries in general

Batteries are energy storing units where electrical energy is stored chemically. When needed, this chemical energy can be converted into electrical energy to power electrical devices such as laptops and mobile phones. A cell, or battery, consists of two electrodes (anode and cathode) separated by an electrolyte and in most instances a separator.

To discharge the cell, the anode and cathode are connected externally to a load as illustrated in figure 2.1. During discharge, the anode material strips electrons from the atoms via oxidation reaction(s). The ions then travel through the electrolyte towards the cathode while the electrons travel through the external circuit to reach the cathode and while doing so power the external load. When the ions and electrons arrive at the cathode they recombine via a reduction reaction. The electrochemical reactions are driven by a potential difference between the electrodes. The process will therefore go on until equilibrium is reached and there is no chemical potential difference between the electrodes [5]. To reverse the process and charge the cell, energy needs to be supplied. The flow of electrons and ions will be reversed and the potential difference between the electrodes increased.

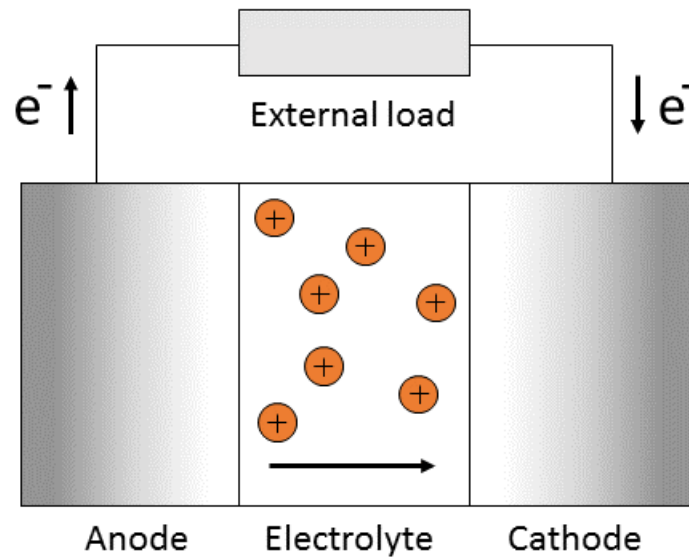


Figure 2.1: Block diagram of a cell powering an external load

2.2 Li-ion batteries

The Li-ion battery (LIB) is common in home electronics. In a LIB lithium ions (Li^+) move between the two electrodes, from the negative to the positive during discharge and opposite during charge.

One example of LIB is based on a lithium cobalt oxide cathod and a graphite anode. After assembly the cell is in a discharged state, with all the lithium in the LiCoO_2 electrode and the corresponding carbon electrode is empty. When charging the cell lithium ions are generated in the positive (LiCoO_2) electrode and move through the electrolyte and go into the negative (carbon) electrode all while the electrons travel through the external circuit. The process follows the reaction stated in equations 2.1 and 2.2. The process is reversed for discharge. The upper arrow indicate discharge and the lower arrow charge. Other Li-ion batteries works in a similar manner.



The theoretical specific capacity for a LIB is around 250-300 mAh/g while the practical specific capacity is not uncommonly more than 100 mAh/g lower, see table 2.1. As the demand on energy storage systems is increasing, the capacity of the LIB is not enough to fill these demands and new Li-based battery technologies are being explored. In the table specific capacities for two commercial cells are presented.

2.3 Li-S batteries

One of the promising battery types to replace the LIB is the lithium-sulfur battery with a theoretical specific capacity of 1675 mAh/g and promise a practical specific

Table 2.1: Specific capacity of lithium batteries

Cathode	Theoretical Specific Capacity [mAh/g]	Practical Specific Capacity [mAh/g]
LiCoO ₂	274	148 [3]
LiMnO ₂	285	140 [3]
S	1675	500-1350 [4]

capacity of 500-1350 mAh/g as seen in table 2.1. The Lithium-Sulfur battery has a sulfur containing cathode. Elemental sulfur is by nature insulating, therefore it needs to be hosted by a conducting material. Due to its abundance and conductivity, the dominating hosting material is porous carbon [6]. The Li-S battery has in most cases a lithium metal anode, unlike the LIB. This comes with some issues such as lithium dendrite formation and low cycling efficiency that reduces cycling life and also effects safety. However, this problem will not be treated in this thesis.

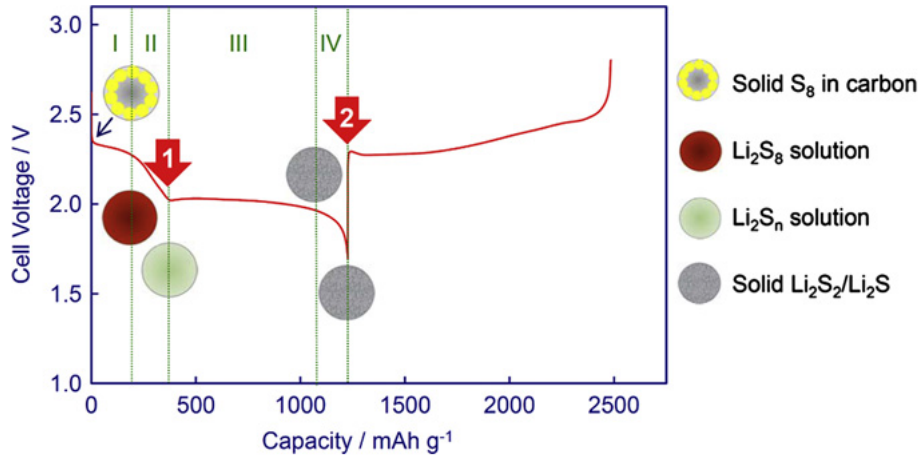
**Figure 2.2:** Typical charge and discharge voltage profiles of a Li-S cell [1].

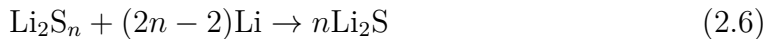
Figure 2.2 shows typical voltage profiles of the charge and discharge of a Li-S cell. During the discharge process elemental sulfur S₈, is reduced to Li₂S in a series of steps where lithium polysulfides are formed, Li₂S_x, (2 < x < 8). The discharge curve can be divided into four regions based on the phase change of polysulfide species. In region I solid elemental sulfur is reduced to Li₂S₈ and dissolved into the electrolyte according to equation 2.3.



The Li₂S₈ is then further reduced in a liquid-liquid phase reduction in region II into lower order polysulfides described in equation 2.4.



In region III two liquid-solid phase reductions compete with each other, as described by equation 2.5 and 2.6. These reactions contribute to the majority of the cells capacity.



Region IV is a solid-solid reduction. This reaction, described by equation 2.7, is slow and suffers from high polarisation. However, if in region III, equation 2.6 would be dominant, region IV would be smaller and the efficiency of the cell would be better. [1]



The lithium polysulfides in these reactions, often called just polysulfides (PS), have a high solubility in the most common electrolytes used. If they are not contained properly by the carbon host, they will dissolve into the electrolyte, which is a major problem. PS in the electrolyte have been shown to be related to problems such as short cycle life, low charging efficiency, poor safety and high self discharge rate [1]. Dissolution of PS in the electrolyte is inevitable and even though efforts are being made to prevent the PS from leaving the carbon host, some PS always leaks out into the electrolyte. Hence it is important to understand the influence of PS dissolution and reactivity of PS in different electrolytes [4], which is the focus of this thesis work.

2.4 Electrolyte

The role of the electrolyte is to connect the two electrodes, to allow the transport of ions from the anode to the cathode. Therefore it must be conductive for that type of ion and non-conducting for the electrons, forcing them to go through the external circuit to reach the cathode. To prevent short circuit of the cell a separator is placed between the electrodes. The separator is soaked in the electrolytes and should not impede the motion of the conductive ions.

An electrolyte is in general made up by an organic solvent and a salt. The salt is essential for the ion transport and the solvents role is to dissolve the salt. To tailor the properties of the electrolyte additional additives can be added [4].

Apart from conducting ions the electrolytes must also fulfil some conditions to make them suitable for the use in a battery. Firstly the electrolyte needs a wide working temperature range [7]. That comes from a low melting point and a high boiling point for the solvent. The addition of lithium salt to the solvent usually increases the working temperature range by decreasing the melting point and increasing the boiling point. Secondly, the electrolyte needs to be thermally stable with a low vapour pressure [7]. In the instance where the electrolyte has a high vapour pressure, the cell might explode and/or catch fire. This must be avoided to all costs, hence it is one of the requirements of the solvent. The electrolyte must also be chemically stable to prevent reactions with the other components in the cell such as the separator or the electrodes [7]. Finally the solvent should have a low viscosity.

The viscosity is intrinsically linked to the conduction of the ions and can depend on the molecular weight and density of the solvent. A low viscosity would also assure complete wetting of the separator and electrodes which is important to utilise all the electroactive materials in the cell [7]. In addition to these physicochemical properties low toxicity and price are commercially important for the choice of electrolyte.

In a perfect world an electrolyte has all these properties, however in the real world that is most likely not the case. When choosing the electrolyte one has to decide what properties that are the most important for the particular application.

2.4.1 Electrode-Electrolyte interface

In the interface between the electrode and the electrolyte a protective layer can be formed as a result of electrolyte decomposition. Some electrolytes form a good layer as is, while other need some additive to help creating it. This layer, referred to as the solid electrolyte interphase (SEI), is formed mainly during the first charge and discharge of the cell and protects the anode by only letting Li-ions through to interact with the anode [8].

2.5 Electrolytes for Li-S batteries

The most common type of electrolyte used for Li-S batteries are non-aqueous organic liquid electrolytes. The most frequently used electrolyte according to a review article from 2014 [4], is the binary mix of 1,3-dioxolane (DIOX) and 1,2-dimethoxyethane (DME), in a 1:1 volume ratio doped with $\approx 1\text{M}$ of the lithium salt lithium bis(trifluoromethanesulfonyl)imide (LiTFSI). Other common electrolyte solvents are glymes (DME or higher molecular weight analogues of DME; DEGDME, TRIEGDME, TEGDME,... etc.). These have been used either pure or in mixtures with DIOX, or ionic liquids.

However, organic solvents have low flash points and high flammability affecting the safety of the batteries negatively [9], hence significant effort is devoted to find alternative solvents. A candidate without these problems is ionic liquids (IL).

2.6 Ionic liquids

Ionic liquids (IL) are salts that are liquid below $100\text{ }^\circ\text{C}$ [10]. An alternative definition for ionic liquids that can be found in literature is salts that are liquid at room temperature or below [11]. In addition to its low melting point ionic liquids can have a liquid phase ranging over $300\text{-}400\text{ }^\circ\text{C}$ before it decomposes [12].

To understand why ionic liquids are different to the typical inorganic salts like NaCl, one can look to the geometry of the salts. The inorganic salts are composed of a large symmetric anion and a smaller symmetric cation as visualised in figure 2.3. The ionic liquids on the other hand are composed of a large anion and a large

asymmetric cation. The lower symmetry together with a delocalised charge lowers the temperature needed for solidification [12].

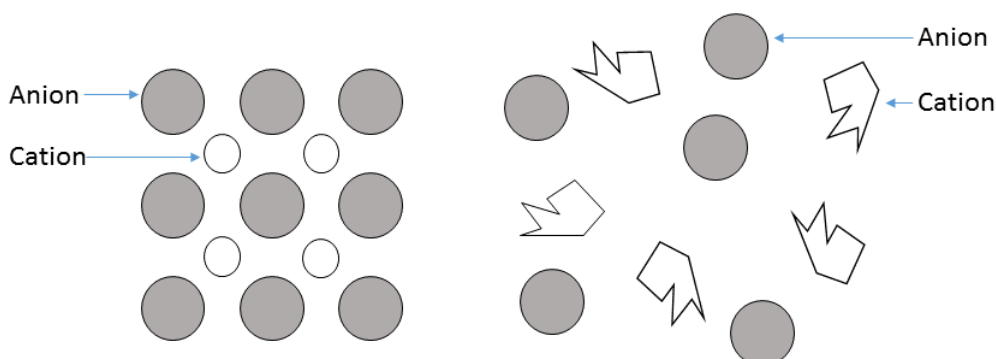


Figure 2.3: The structure of a typical inorganic salt to the left and an ionic liquid to the right.

There is a large number of anions and cations available which makes it possible to tune the properties of the ionic liquid [12].

2.6.1 Ionic liquid as an electrolyte solvent

Unlike organic solvents ionic liquids have high thermal stability and are nonflammable. In addition to this ILs have high ion conductivity, a large electrochemical stability window and good solubility for many Li-salts [4]. However, as mentioned in section 2.4 it is unlikely for a solvent to have all the desired properties of an electrolyte. The drawbacks of ILs are that they have higher viscosity and are, so far, more expensive than the organic solvents [4].

With ionic liquid based electrolytes for lithium-sulfur batteries the safety would increase compared to electrolytes based on organic solvents. Still, the problem with the polysulfides remains to be investigated and understood.

3

Theory

3.1 DSC

Differential scanning calorimetry (DSC) is a method used to study phase transitions based on the generation or consumption of heat. By measuring the change of the difference in heat flow between the sample and a reference while keeping the surrounding temperature controlled, one can detect phase transitions such as melting and glass transitions within the sample [13].

3.1.1 DSC data

To visualise the result of a DSC measurement the heat flow is plotted as a function of temperature see figure 3.1. An endothermic reaction, such as melting, need a supply of energy and would then, assuming exothermic reactions is indicated as up in the figure, result in a dip in the heat flux. The opposite is true for exothermic reactions such as crystallisation where energy is released creating a peak in the heat flux. The temperatures at the corresponding minimum/maximum of the peaks are used as crystallisation temperature (T_x) and melting temperature (T_m) respectively. A glass transition, where a material goes from a glass to a liquid, shows as a step in the heat flow data [14]. The glass transition is not an instantaneous transition at an exact temperature like for example the melting point. It has an onset and an endset temperature where the glass transition takes place. In this thesis the glass transition temperature, T_g will be defined as the midpoint of the transition. All discussed transitions can be seen in figure 3.1 where the inset is a magnification of the region where the glass transition takes place.

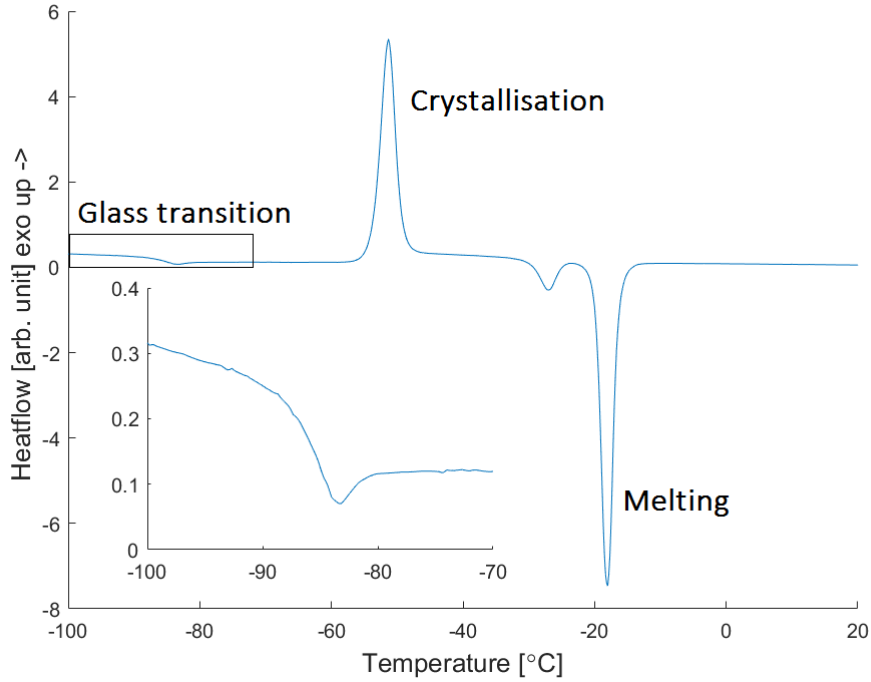


Figure 3.1: DSC trace for P14TFSI showing glass transition, crystallisation and melting. The inset show a magnified image of the trace in the square.

3.2 Ionic conductivity

Ionic conductivity describes how well ions are transported in a medium. The ionic conductivity depends on the concentration and mobility of the ions, valence of the ions and the temperature.

The ionic conductivity is measured by applying an alternating electrical current between two electrodes separated by the sample and then measure the voltage response. The resistance can then be calculated using Ohm's law. From that the conductivity (σ [Scm^{-1}]) is calculated with equation 3.1,

$$\sigma = \frac{1}{R} \frac{d}{a} \quad (3.1)$$

where R , d and a is the electrical resistance [Ω], the distance between the probe electrodes [cm] and the effective area of the electrodes [cm^2] respectively.

The ionic conductivity is the sum of the individual contributions by each ion type in a sample.

$$\sigma_{total} = \sum_i \sigma_i \quad (3.2)$$

Complementary techniques are therefore required to determine the contribution of each specific ion.

3.3 NMR

Nuclear magnetic resonance (NMR) spectroscopy uses the interaction of electromagnetic radiation of radiofrequency with nuclei in a strong magnetic field to study the local structure and motion of molecules.

A nuclei with a net spin placed in a strong, uniform magnetic field, H_0 , will have its magnetic dipole quantized into a discrete set of orientations corresponding to different energy levels. The energy levels are equidistant and the energy difference is given by equation 3.3

$$\Delta E = \gamma \hbar H_0 \quad (3.3)$$

where γ , \hbar and H_0 is the gyromagnetic ratio, planks constant divided by 2π and the applied magnetic field respectively. When the system is in thermal equilibrium the spins follow a Boltzmann distribution as in equation 3.4. N_{upper} and N_{lower} describe the number of spins in the higher and lower energy states.[15]

$$\frac{N_{upper}}{N_{lower}} = \exp(-h\nu/Tk) \quad (3.4)$$

Using the Bohr condition, $\Delta E=h\nu$, the frequency (ν) corresponding to this energy difference can be expressed as in equation 3.5.

$$\nu = \frac{\gamma H_0}{2\pi} \quad (3.5)$$

For a given magnetic field, this frequency is characteristic for a particular nuclei, because of the characteristic of the gyromagnetic ratio [15]. However this assumes no other magnetic field interferes with the applied one, which most of the time is not the case. Surrounding electrons cause an induced magnetic field opposed to the applied field. The effective field that affects the nucleus is then $H_{eff} = H_0 - a H_0$ where a is a non-dimensional constant for the amount of screening and together with H_0 describes the strength of the screening field induced by surrounding electrons. Consequently, H_0 has to be replaced by H_{eff} in equation 3.5, resulting in a lower characteristic frequency. If this frequency is applied to the system in a pulse long enough all spins will be excited. When the pulse ends the spins start to relax back to equilibrium and the emission photons are registered. From the molecular structure and electron density of a molecule one can then detect what signal comes from what nucleus. The technique is limited to nucleus with a net spin, hence only molecules including nucleus such as ^1H , ^2H , ^7Li , ^{13}C , ^{15}N , and ^{19}F can be studied.

3.3.1 PFG spin-echo

In order to investigate self-diffusion of molecules in a sample the diffusion coefficient can be measured. Using pulsed field gradient (PFG) spin-echo, a specific NMR technique, where a gradient pulse with strength G and length δ is applied to the system to map the nuclei. After the pulse, the system is left to self-diffuse for time Δ after which a new pulse is sent to map the nuclei. Only the nuclei that haven't

moved during the diffusion time is registered. This procedure is then repeated while either G , δ or diffusion time (Δ) is varied to gather data for the fitting. The diffusion coefficients of the nuclei in the sample can be determined by fitting data to equation 3.6.

$$I_G = I_0 \exp \left(-D(\gamma\delta G)^2 \left(\Delta - \frac{\delta}{3} \right) \right) \quad (3.6)$$

Where I_0 , D , γ , G , δ and Δ is reference intensity, diffusion coefficient, gyromagnetic ratio, gradient strength, length of gradient and diffusion time respectively [16]. The area under the peaks is used as intensity in equation 3.6 from where the diffusion coefficient can be decided [16].

Diffusion coefficients (D) are related to the mobility (μ) as described in equation 3.7 [17], where k_B is Boltzmanns constant and T is the temperature, and is therefore a good measure of the mobility of molecules which in turn is related to the ionic conductivity.

$$D = \mu k_B T \quad (3.7)$$

3.4 Impedance

Impedance is the counterpart of resistance for AC circuits. It is a complex value calculated using Ohms law,

$$U = Z \cdot I \quad (3.8)$$

where U is the complex voltage, Z is the complex impedance and I is the complex current. To measure the impedance a sinusoidal voltage is applied to the sample and the current response is measured. The phase difference between the applied and measured reponse is used to calculate the impedance.

3.4.1 EIS

Any electrochemical system can be modelled as an equivalent electrical circuit where the different parts of the system are replaced by resistances and capacitors. These components can be reduced into one, frequency dependent, impedance. Hence, different parts of the system, such as the electrolyte, or the SEI, respond differently depending on the frequency. This is used in electrochemical impedance spectroscopy (EIS) where a sinusoidal voltage is applied for a range of different frequencies to investigate the impedance of the different components of the system.

One way of plotting the data from an EIS experiment is in a Nyquist diagram see figure 3.2. The real value of the impedance is plotted on the x-axis against the negative imaginary value of the impedance on the y-axis where every point is the impedance for one particular frequency. The frequency decreases along the x-axis.

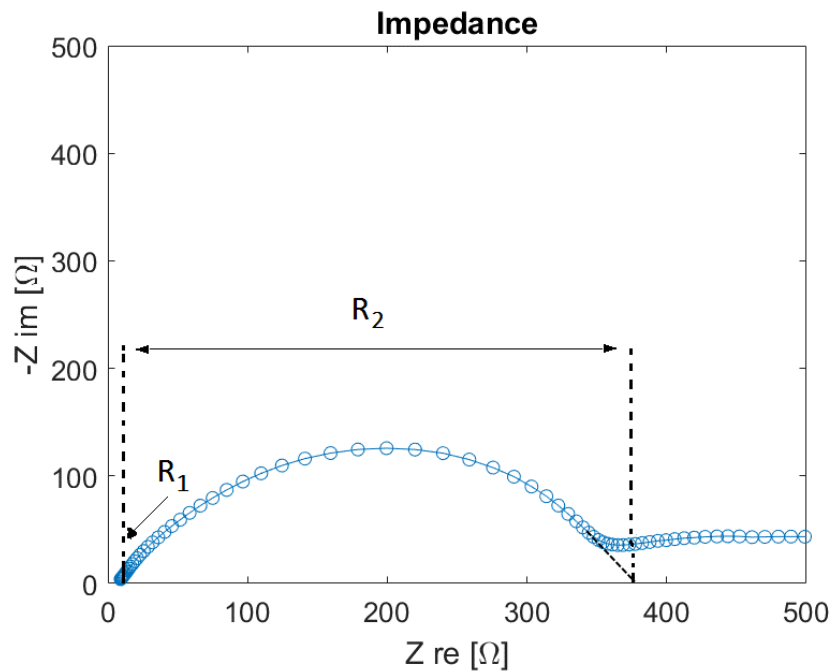


Figure 3.2: Nyquist plot from an impedance experiment. The resistance of the electrolyte (R_1) and the SEI (R_2) are indicated in the figure.

3.4.2 EIS to show SEI formation

Impedance measurements can be used to track the SEI formation on electrodes. To do this a cell where both electrodes are lithium (symmetrical cell) can be used. Right after assembly the pristine cell can be described by the left part of figure 3.3. When the electrolyte is in contact with the lithium metal, the electrolyte will decompose as described in section 2.4.1 creating a SEI as shown to the right in the figure. As the SEI evolves the impedance of the cell will change. By conducting impedance measurements at various intervals for a cell with resting time between, one can track the formation of the SEI by its resistance. The first x-intercept, in the high frequency region, describes the resistance of the electrolyte and the separator [18]. The second x-intercept of the semi circle in the high to medium frequency region represent the resistance of the two SEI layers [19] as seen in figure 3.2. The corresponding electrical current for such a cell could simplified be described as in figure 3.4, where R_1 is the resistance of the electrolyte and R_2 is the resistance of the SEI layers.

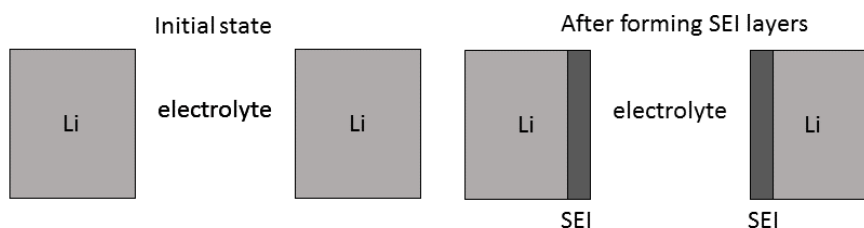


Figure 3.3: SEI formation in a symmetrical cell

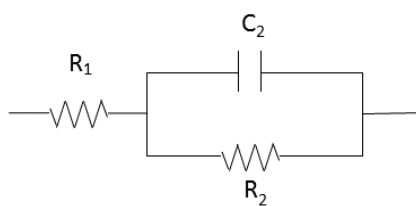


Figure 3.4: Equivalent electrical circuit of a symmetrical cell with an SEI

3.5 Cycling of symmetrical cells

When applying a constant current to a symmetrical cell, both electrodes are lithium, the voltage response measured can be used to calculate the resistance of the full cell using Ohm's law. When charging and discharging the cell, by drawing a current in different directions, Li is stripped from one electrode and plated on the other.

4

Experimental methods

4.1 Sample preparation

In this study two different kinds of ionic liquids were used as solvents. The first ionic liquid was 1-Propyl-1-methyl-pyrrolidinium Bis(fluorosulfonyl)imide, P13FSI for short, where 1-Propyl-1-methyl-pyrrolidinium (P13) is the cation and Bis(fluorosulfonyl)imide (FSI) is the anion bought from Wuhan. The second ionic liquid used was 1-Butyl-1-methyl-pyrrolidinium Bis(trifluoromethanesulfonyl)imide, P14TFSI for short, with a 1-Butyl-1-methyl-pyrrolidinium (P14) cation and a Bis(trifluoromethanesulfonyl)imide (TFSI) anion bought from Iolitec. As salt for the two ionic liquids their corresponding anion lithium salt was used. The LiFSI was bought from Boulder Ionics and the LiTFSI was bought from 3M. All of the chemical structures are shown in figure 4.1.

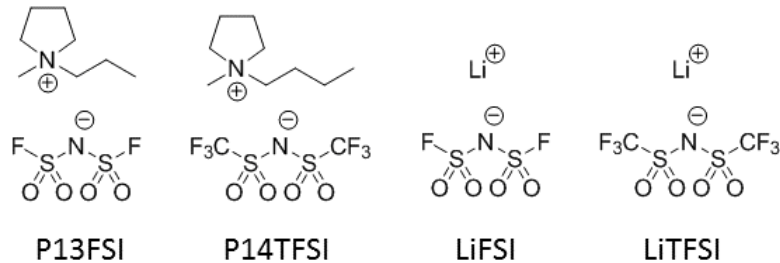


Figure 4.1: Molecular structures of P13FSI, P14TFSI, LiFSI and LiTFSI

Apart from the lithium salt, polysulfides (PS) were also added to the ionic liquids, as this study aims to investigate how the addition of polysulfides change the properties of the electrolyte. The chemicals used to form these PS, Li_2 and S_8 , were purchased from Sigma Aldrich. Polysulfides are easily produced by mixing Li_2S and S_8 . Depending on the ratio between Li_2 and S_8 one gets different polysulfides, according to the relation



Because of the varying solubility of different PS the, Li_2S_4 , Li_2S_6 and Li_2S_8 was tested. Li_2S_4 and Li_2S_6 were found to be the easiest to dissolve and therefore chosen for this study.

When investigating the maximum solubility of polysulfides the ionic liquid P14TFSI

was used as solvent and Li_2S_4 as the polysulfide. The PS concentration was varied from 1 mol/kg and down to a concentration where everything dissolved. The maximum solubility was found to be around 0.04 mol/kg solvent. To make sure also the Li-salt would dissolve 0.02 mol/kg was used as PS concentration and 0.1 mol/kg was used for the Li-salt. The different compositions of the samples used in the study are presented in table 4.1.

Table 4.1: Compositions of the samples investigated

Components	A	B	C	D	E	F	G	H	I	J	K	L
P13FSI	x	x	x	x	x	x						
P14TFSI							x	x	x	x	x	x
0.1 mol/kg LiFSI		x			x	x						
0.1 mol/kg LiTFSI								x			x	x
0.02 mol/kg Li ₂ S ₄			x		x				x		x	
0.02 mol/kg Li ₂ S ₆				x		x				x		x

The samples were prepared in an argon filled glovebox. Ionic liquid was weight in a vial and the amounts of polysulfides and lithium salt were calculated thereafter. The desired PS was obtained by mixing Li_2S and S_8 in another vial according to equation 4.1 and crushed together with a spatula. For the samples with Li-salt, the salt was added at the same time. The ionic liquid was then added to the mix and the vial was put on a hot plate at 60 °C to dissolve overnight.

4.2 Phase transitions - DSC

For a battery it is, as mentioned in section 2.4, important for the electrolyte to stay liquid in a large temperature range. It is therefore interesting to investigate if the electrolyte shows a melting point and/or a glass transition and how that changes upon addition of PS to the electrolyte. This is easily determined by DSC.

Approximately 4-6 mg of each sample was put in an aluminium crucible that was sealed properly in a glove box. The crucibles were pierced before analysis to prevent any possible pressure build up. For the P13FSI based samples the analysis was performed with a Mettler Toledo DSC 3 with Huber Intra cooler. The samples were cooled down to -70 °C and then heated at 10 °C/min up to 150 °C under N_2 purge gas at 40 mL/min.

To show a melting point for all P14TFSI based samples a faster cooling rate had to be used for these samples, therefore a Mettler Toledo DSC 3 system equipped with Liquid Nitrogen cooling was used for those measurements. The crucibles were cooled at 20 °C/min down to -120 °C where the temperature was held for 5 minutes before it was increased again 10 °C/min until it reached 150 °C. This was done under N_2 purge gas at 40 mL/min.

4.3 Ionic conductivity

For batteries it is important that the ionic conductivity is high and doesn't change too much when temperature changes as this directly impacts on the charge/discharge rate of the device. Hence, the ionic conductivity was measured. However, the time of the project was not enough to do investigate the temperature dependence.

The samples were filled up in a glass tube and the dip probe was lowered into the liquid. The ionic conductivity was measured using a Mettler Toledo SevenMulti instrument at 25 °C. All sample preparation was performed in a glove box.

4.4 Diffusion coefficients

The self diffusion of the different molecules in the samples were investigated using PFG spin-echo NMR to reveal how the mobility of the molecules change upon adding lithium salt and polysulfides.

Three nuclei were investigated, ^1H , ^{19}F and ^7Li each of them representing a component of the electrolyte. Figure 4.1 shows the molecular structure of the components of the electrolyte. The only ion in the sample containing hydrogen is the cation, hence the signal from the hydrogen can be used to describe the properties of the cation. Using the same reasoning the fluorine signal represents the anion. The Li-signal will represent the free lithium ions.

The NMR-tubes were filled, 4-5 cm, in the glove box, sealed and transferred to the NMR-instrument. NMR diffusion coefficients were determined using the PFG spin-echo method utilising a Bruker Av400 NMR spectrometer equipped with a 5 mm broadband BB-H/D probe operating at 400.13 MHz for ^1H with a 5.35 G/mm z-gradient. Bruker's software, TopSpin 3.5.7, was used for acquisition and processing of the data.

Samples were investigated at 20, 40, 60 and 80 °C (± 0.1 °C). At least 30 minutes was allowed for each sample to reach thermal equilibrium at each temperature before any measurements were made. The NMR data were measured with a stimulated echo sequence with one spoil gradient; the diffusion time (Δ) was 100 ms and the gradient pulse length (δ) was 10 ms for all measurements; gradient pulses were smoothed square chirp shape.

Experiments were performed as pseudo-2D with a linear variation of the gradient from 2 to 95% of maximum intensity in 32 steps. The data were processed and the peak areas, I , were used to fit equation 3.6 to the data to determine the diffusion coefficient, D , as single component fits.

4.5 SEI

For long time cycling of Li-S batteries it is important that a stable SEI is formed on the lithium anode. Using impedance measurements and cycling data of symmetrical cells one can investigate the resistivity of the cell and how it changes during cycling.

4.5.1 Symmetrical cell assembly

In figure 4.2 a schematic over the assembly of a symmetrical Li|electrolyte|Li cell is shown. The cells were assembled as coin cells, starting with the stainless steel bottom part of the housing. A plastic ring was placed in the bottom to help seal the cell properly. A 12 mm (diameter) wide and 0.4 mm thick lithium metal electrode was placed in the housing. 20 μl electrolyte was dropped onto the electrode and then covered with a 15.9 mm in diameter wide Whatmann glass fibre separator. On top of the separator 70 μl electrolyte was applied before the second electrode was placed in the cell. Thereafter a metal spacer and a metal spring was put in the cell and finally the top part of the housing was added and the cell was sealed. The cell assembly was done in a glove box.

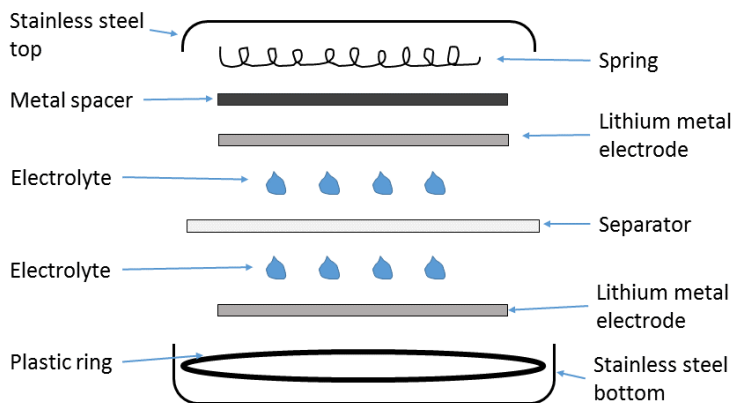


Figure 4.2: Cell components of a symmetrical cell

4.5.2 Impedance

The impedance was measured in a frequency range of 100 kHz - 100 mHz on a Solatron 1255B analyser within an hour of assembly before the first cycles and then after every 20 cycles.

4.5.3 Cycling

The symmetrical cells were cycled in 3 rounds of 20 cycles each on a series 4000 Maccor battery tester using following program:

Rest 1 minute

for *20 times* **do**

 Charge at constant current for 16 minutes

 Rest 30 sec

 Discharge at constant current for 16 minutes

 Rest 30 sec

end

The first round was run with 0.1 Ah/cm^2 , the second run with 0.25 Ah/cm^2 and the third round 0.1 Ah/cm^2 again.

To keep the temperature stable during the cycling the cells were kept in an isolated box.

5

Results and discussion

5.1 Solubility of Polysulfides in Ionic Liquid

Figure 5.1 and 5.2 shows the final solutions used in the study, 0.1 mol/kg lithium salt and 0.02 mol/kg polysulfides. Since the solubility was tried out on what turned out to be the easiest dissolved PS in pure IL many of the other samples have a small amount of (what is assumed to be) undissolved sulfur floating on the surface. Thus, the concentration of polysulfides in these samples is slightly lower than stated.

The P14TFSI based samples to the right show the characteristic reddish colour of polysulfides dissolved in electrolytes. The P13FSI electrolytes to the left on the other hand have a different appearance. One can visually see a clear difference in the solubility between the samples with only PS (C and D) and the ones with PS and lithium salt (E and F). In samples C and D the PS are dissolved, with some particles on the surface of the Li_2S_6 sample, however in samples E and F the PS are hardly dissolved at all.

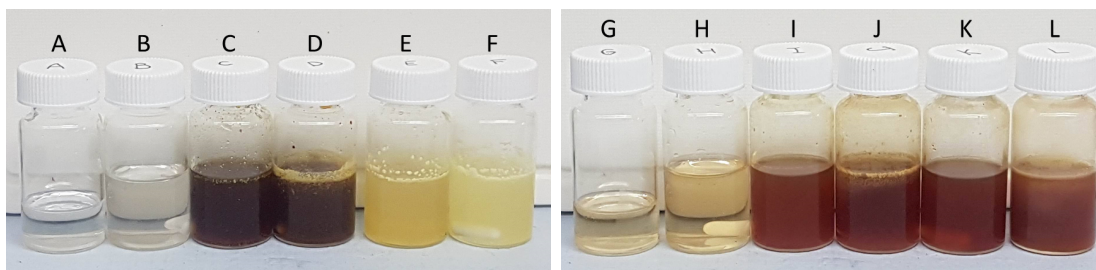


Figure 5.1: P13FSI based samples

Figure 5.2: P14TFSI based samples

Table 5.1: Sample compositions

Components	A	B	C	D	E	F	G	H	I	J	K	L
P13FSI	x	x	x	x	x	x						
P14TFSI							x	x	x	x	x	x
0.1 mol/kg LiFSI		x			x	x						
0.1 mol/kg LiTFSI								x			x	x
0.02 mol/kg Li_2S_4			x		x				x		x	
0.02 mol/kg Li_2S_6				x		x				x		x

5.2 DSC

For a battery it is, as mentioned in section 2.4, important for the electrolyte to stay liquid in a large temperature range. It is therefore interesting to investigate if the electrolyte show a melting point and/or a glass transition and how that changes upon addition of PS to the electrolyte. This is easily determined using DSC.

The DSC results for the P13FSI based electrolytes show no bigger differences for the different compositions as shown in figure 5.3 and the values for the thermal transitions are presented in table 5.2. The DSC traces in the figure show two endothermic transitions around $-18\text{ }^{\circ}\text{C}$ and $-9\text{ }^{\circ}\text{C}$. These values agree within a few degrees with previous studies done on pure P13FSI by Zhou *et al.* [20] and Yoon *et al.*[21] where they report the first peak to be a solid-solid phase transition and the second peak to be the melting. No glass transition is observed for the P13FSI samples. Zhou *et al.* tried to force a glass transition by cooling P13FSI at $40\text{ }^{\circ}\text{C}/\text{min}$ but even then the sample crystallised [20]. Huang and Hollenkamp investigated the phase transitions P13FSI with varying concentrations of LiFSI and only for concentration of 0.5 mol/kg and more a glass transition was observed [22].

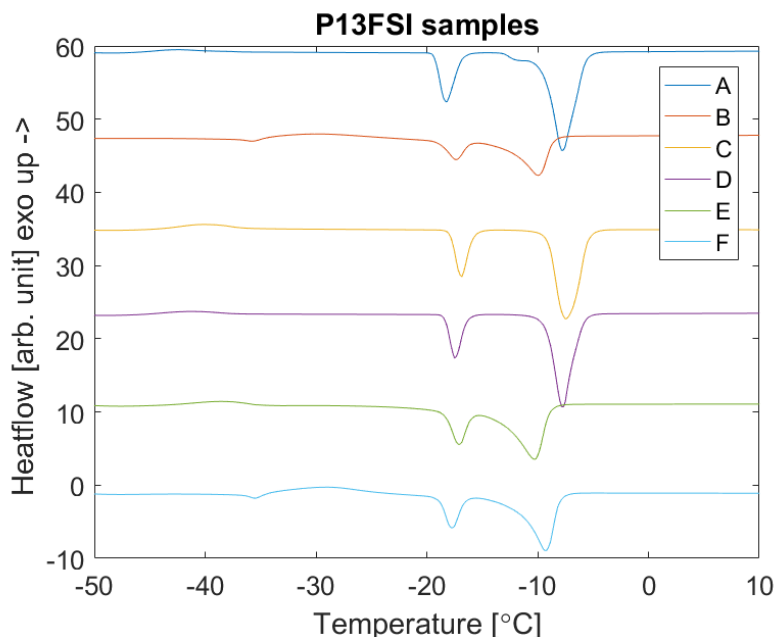


Figure 5.3: DSC-traces of P13FSI based electrolytes

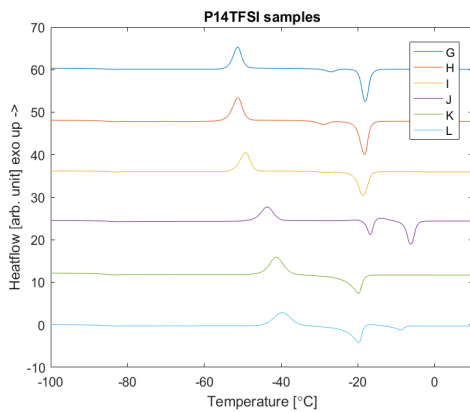
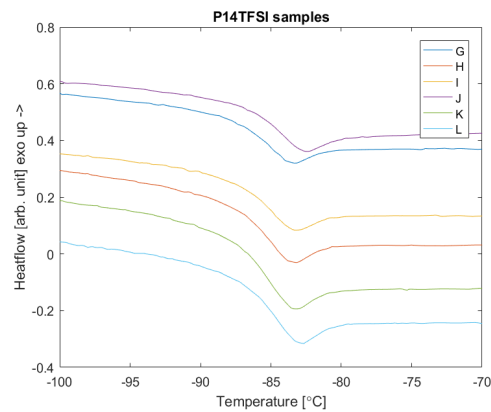
The results from the DSC measurements on the P14TFSI based electrolytes are shown in figure 5.4 and the values for the thermal transitions are presented in table 5.3. All samples show a glass transition, crystallisation and melting. A zoomed in image of the region where the glass transition occurs is found in figure 5.5, where a clear change in the heat flow is observed for all samples. The glass transition occurs around $-84\text{ }^{\circ}\text{C}$ for all the samples. This value was calculated as the mean value of the onset and the endset temperatures provided by the DSC-software. Martinelli *et al.* [23] report a glass transition at $-81\text{ }^{\circ}\text{C}$ which is slightly higher than the one

Table 5.2: Temperatures for thermal transitions in the P13FSI based electrolytes

Sample	$T_{solid-solid}$ [°C]	T_m [°C]
A	-18	-8
B	-17	-10
C	-17	-8
D	-18	-8
E	-17	-10
F	-18	-10

observed here.

Two endothermic peaks are found for all P14TFSI-based electrolytes but the ones with added Li_2S_4 (I and K), where the second of the two peaks is the melting. MacFarlane *et al* observed two endothermic peaks for pure P14TFSI, the first at -24 °C described as a solid-solid transition just as in the P13FSI case, and the second peak at -18 °C as the melting [24]. These values agree with the values measured for the pure P14TFSI and when the Li-salt is added where a melting temperature of -18 °C was found. However, when the Li_2S_4 is added the first peak disappears showing just one peak with a T_m around -19 °C. Upon addition of Li_2S_6 to the electrolyte the two endothermic peaks shift, increasing the melting temperature with about 10 degrees to -6 °C for the electrolyte with only Li_2S_6 and -9 °C when the Li-salt is also present.

**Figure 5.4:** DSC-traces of P14TFSI based electrolytes**Figure 5.5:** DSC-traces showing the glass transition for P14TFSI based electrolytes.

Another difference in the DSC-traces for the different electrolytes is the crystallisation peak. As the polysulfides are introduced to the electrolyte T_x shifts more than 10 °C from -51 °C in the sample with IL and LiTFSI to -40 °C when Li_2S_6 is added.

Table 5.3: Temperatures for thermal transitions in P14TFSI based electrolytes

Sample	T_g [°C]	T_x [°C]	T_m [°C]	$T_{endothermic}$ [°C]
G	-85	-51	-18	-27
H	-84	-51	-19	-29
I	-84	-49	-19	
J	-83	-44	-6	-17
K	-84	-41	-20	
L	-86	-40	-9	-20

5.3 Ionic conductivity

The conductivities measured for the different electrolytes are tabulated in table 5.4. The electrolytes containing sulfur were filtered before the experiment, in order to remove undissolved sulfur particles floating on the surface of some of the samples. The filtration was done through a PVDF membrane in a Millex-HV filter with 0.45 μm sized pores. For the following discussion all lithium salt is assumed to be dissolved and that only PS was removed when the samples were filtered.

The pure P13FSI has a conductivity of 8.7 mS/cm. Similar conductivities have been presented by Ishikawa *et al.* and Matsumoto *et al.*, that presented 8.3 mS/cm [25] and 8.2 mS/cm [26] respectively. Solvionic present the conductivity of P14TFSI to be 2.8 mS/cm at room temperature [27], which agree well with the presented value in table 5.4.

Even though there is a clear difference in the conductivity between the two ionic liquids the ionic conductivity follow similar trends when Li-salt and PS are added. One can see a conductivity drop for both ILs when the corresponding Li-salt is added which is expected since dissolution of a $[\text{Li}^+][\text{X}^-]$ salt in a $[\text{A}^+][\text{X}^-]$ ionic liquid leads to a lowered conductivity [28]. The conductivity is also lowered when PS is added to the pure ionic liquid, however the change is much smaller.

When the PS is added to the electrolyte (IL and Li-salt) the conductivity of the two ionic liquids changes differently. The P13FSI-based electrolytes show an increased conductivity when PS are added, while the conductivity for the P14TFSI based electrolytes decreases. The results seem to be indifferent to the type of PS present in the electrolyte.

Table 5.4: Ionic conductivity at 25 °C

P13FSI	Conductivity [mS/cm]	P14TFSI	Conductivity [mS/cm]
A	8.7	G	2.7
B	8.1	H	2.3
C	8.6	I	2.6
D	8.6	J	2.6
E	8.2	K	2.1
F	8.3	L	2.1

5.4 NMR

Since the diffusion coefficient is proportional to the mobility, the two will be used interchangeably in the following discussion. Diffusion coefficients for all samples measured at 20 °C are shown in figure 5.6. The diffusion coefficients at 40 °C, 60 °C and 80 °C show the same features and can be found in appendix A.1. All diffusion coefficients are different, suggesting that the ions move independently of each other. For the P13FSI samples the anion is more mobile than the cation, in contrast to the P14TFSI samples, where the cation show higher mobility than the anion. For both samples the Li-ion mobility is the lowest.

When LiFSI is added to the P13FSI it causes a large drop in the diffusion coefficient for both the anion and the cation. The diffusion coefficient of the anion and cation in sample C and D is lower than in the pure P13FSI, showing a slightly higher mobility for the anion and cation for the Li_2S_6 PS. However when both LiFSI and PS are dissolved in the sample the mobility of the anion and cation is just slightly higher than for the sample with only salt. There one can also observe a higher anion/cation mobility for the Li_2S_4 sample rather than the Li_2S_6 as was without the LiFSI. Adding the PS to the lithium salt result in a mobility increase for the Li, where the mobility is higher when Li_2S_4 is added compared to Li_2S_6 .

Unfortunately the signal was too low for the P13FSI samples with only Li_2S_x to determine the diffusion coefficient. Two possible reasons could be that the relaxation was too fast for the instrument or that the probed nucleus (Li) in the sample were undissolved (too low concentration). The colour of the solution however indicates that the PS indeed are dissolved.

For the P14TFSI samples one observes a drop in diffusion coefficient for the anion/cation when LiTFSI is added to the IL, just as in the corresponding P13FSI electrolytes, but the change is comparatively smaller. For the samples with P14TFSI and PS a higher mobility for the anion/cation is shown in the sample with Li_2S_6 compared to Li_2S_4 . When the PS is introduced to the LiTFSI sample the anion/cation mobility is decreased, with a slightly higher mobility in the Li_2S_6 sample. The mobility of lithium in the solution is high for the sample with P14TFSI and LiTFSI. For the samples with PS the mobility is slightly lower and a higher Li mobility

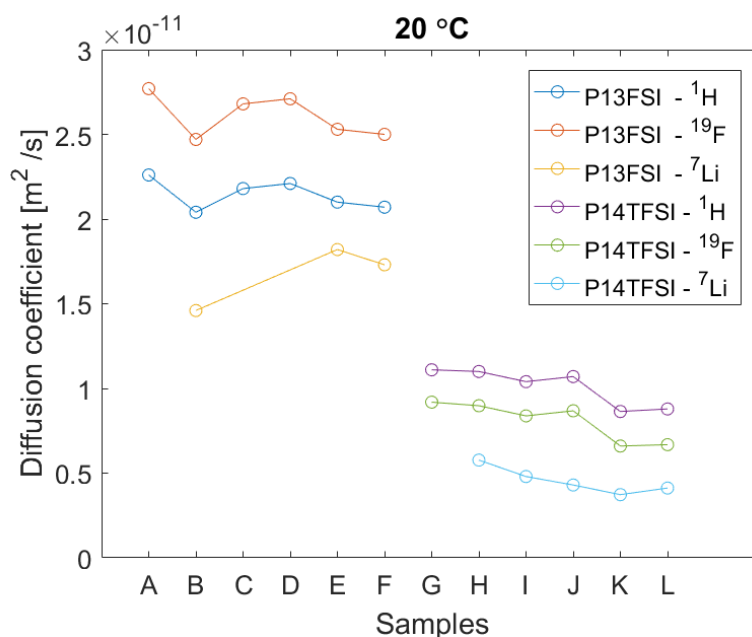


Figure 5.6: Diffusion coefficients at 20 °C

is observed for the Li_2S_4 sample. However when the salt is added the highest Li mobility is seen in the Li_2S_6 sample instead.

5.5 Impedance

The impedance measured for symmetric cells with pure P13FSI and pure P14TFSI is plotted in Nyquist diagrams in figure 5.7 and 5.8 respectively. A clear difference in impedance can be observed between the two ionic liquids in line with the conductivity measurements. Nyquist plots for all samples can be found in Appendix A.2.

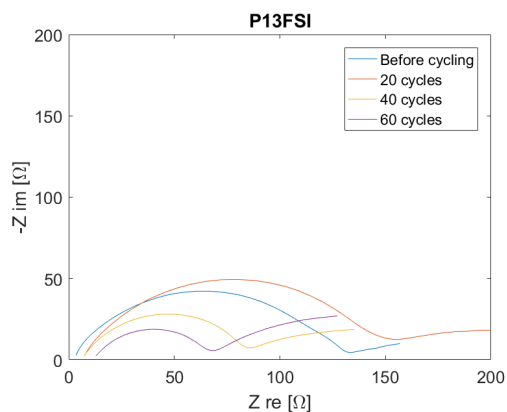


Figure 5.7: Nyquist plot of impedance for P13FSI

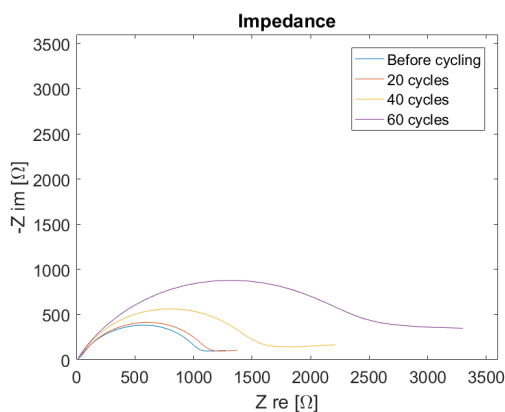


Figure 5.8: Nyquist plot of impedance for P14TFSI

To visualise the formation of the SEI over time, the resistance of the SEI is plotted

as a function of cycle number in figure 5.9 for the P13FSI based samples and in figure 5.10 for the P14TFSI based samples. The resistance was decided as described in section 3.4. A visual estimation of the second intercept with the x-axis was done, error bars are provided in the figure but are contained within the size of the markers.

The impedance of the final SEI layer after 60 cycles for the P13FSI based cells are all lower than the initial impedance except for the sample with IL and Li-salt. Adding LiFSI to P13FSI seem to inhibit a stable SEI of forming. Adding PS to the electrolyte on the other hand seems to help forming the SEI layer. Similar results are shown for all samples with PS with or without the LiFSI.

The P14TFSI electrolytes also seem to form a stable SEI layer during cycling. Pure P14TFSI however does not. The impedance just keep growing during cycling. For the rest of the samples the final impedance is slightly higher than the initial one, and shows no bigger differences for the different compositions.

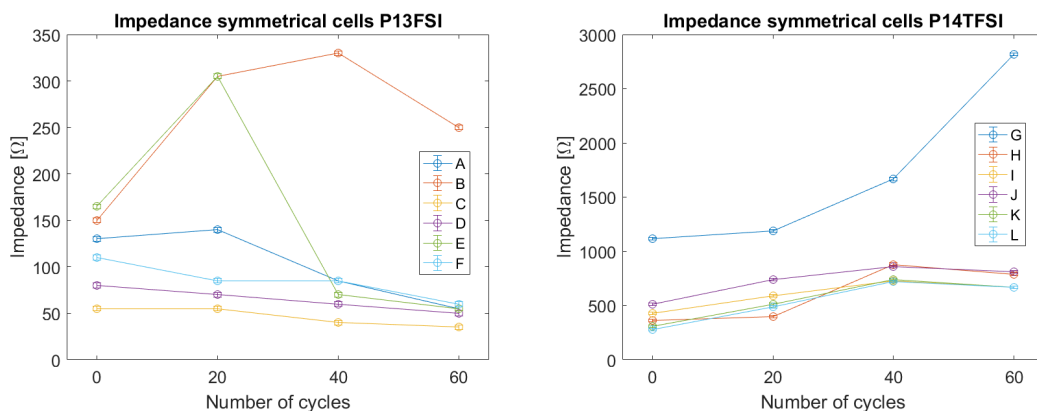


Figure 5.9: Impedance of symmetric cells with P13FSI based electrolytes as a function of cycle number

Figure 5.10: Impedance of symmetric cells with P14TFSI based electrolytes as a function of cycle number

5.6 Cycling

The voltage changes over time for the cycling of the symmetrical cells with P14TFSI and LiTFSI as electrolyte is plotted in figure 5.11. The inset is a magnification of the first two cycles. Voltage profiles of all the cycled cells are found in appendix A.3. When comparing the P13FSI based and the P14TFSI based samples one can see a clear difference in voltage, in agreement with the impedance and conductivity measurements.

The resistance calculated from the voltage profiles and the resistance from the impedance measurements are compared in figure 5.12. The resistance was calculated using the peak value of the voltage of the last cycle. To get an as good comparison as possible between the DC cycling and the AC impedance measurement

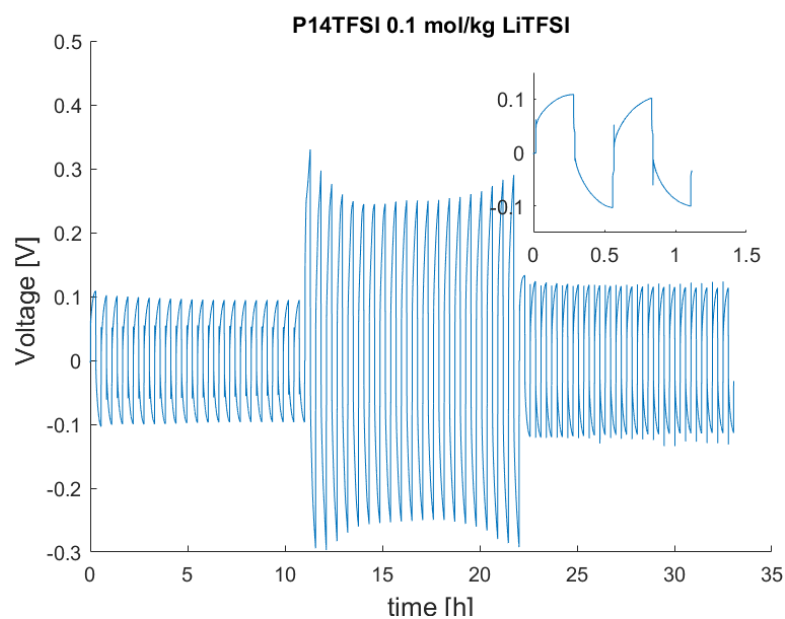


Figure 5.11: Voltage profile for P14TFSI electrolyte. Inset is a magnification of the first two cycles.

the impedance with the lowest frequency (0.1 Hz) was used. Despite the frequency difference in the comparison, the resistances are in good agreement.

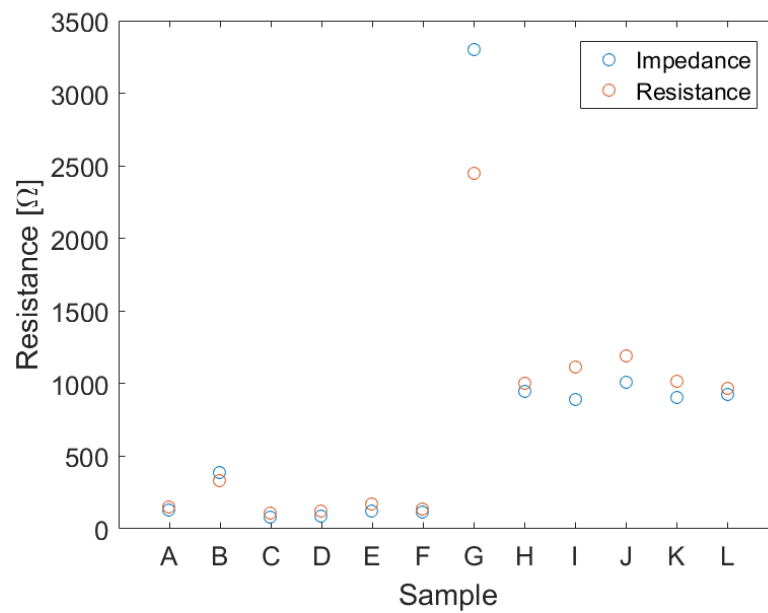


Figure 5.12: Comparison of resistance measured from impedance and cycling data.

6

Conclusion

This study has shown that for the low concentrations of PS used here, the PS does not affect the investigated properties considerably. For its application as Lithium-Sulfur batteries this is the wanted outcome.

However what was found is that the melting temperature and other endothermic transitions for P13FSI electrolytes is unaffected upon adding of PS. For the P14TFSI electrolyte the presence of PS increases the crystallisation temperature while the melting temperature increases for addition of Li_2S_6 but not for the Li_2S_4 . The glass transition however is more or less unaffected.

Upon adding of PS the two ionic liquids respond differently in terms of conductivity. Adding PS to a P13FSI electrolyte increases the conductivity while it decreases for P14TFSI, seemingly indifferent to the type of PS.

Consistent results are shown for the diffusion coefficients, where the mobility increases for anion, cation and lithium-containing molecules when PS is added to the P13FSI electrolyte. For P14TFSI on the other hand the mobility decreases upon adding of the PS to the electrolyte.

Polysulfides dissolved in the P13FSI based electrolyte helps forming a stable low resistance SEI. Adding PS in P14TFSI based electrolyte does not affect the resistance of formation of the SEI.

Bibliography

- [1] Sheng S. Zhang. Liquid electrolyte lithium/sulfur battery: Fundamental chemistry, problems, and solutions. *Journal of Power Sources*, 231:153 – 162, 2013.
- [2] Model s - range per charge. <https://www.tesla.com/models>. Accessed: 2017-06-28.
- [3] Naoki Nitta, Feixiang Wu, Jung Tae Lee, and Gleb Yushin. Li-ion battery materials: present and future. *Materials Today*, 18(5):252 – 264, 2015.
- [4] Johan Scheers, Sébastien Fantini, and Patrik Johansson. A review of electrolytes for lithium–sulphur batteries. *Journal of Power Sources*, 255:204 – 218, 2014.
- [5] Koji Nishio and Nobuhiro Furukawa. *Practical Batteries*, pages 27–85. Wiley-VCH Verlag GmbH & Co. KGaA, 2011.
- [6] Linda F. Nazar, Marine Cuisinier, and Quan Pang. Lithium-sulfur batteries. *MRS Bulletin*, 39(5):436–442, 2014.
- [7] Wu Yuping. *Lithium-Ion Batteries: Fundamentals and Applications*, volume 4. CRC Press, 2015.
- [8] Magali Gauthier, Thomas J. Carney, Alexis Grimaud, Livia Giordano, Nir Pour, Hao-Hsun Chang, David P. Fenning, Simon F. Lux, Odysseas Paschos, Christoph Bauer, Filippo Maglia, Saskia Lupart, Peter Lamp, and Yang Shao-Horn. Electrode–electrolyte interface in li-ion batteries: Current understanding and new insights. *The Journal of Physical Chemistry Letters*, 6(22):4653–4672, 2015. PMID: 26510477.
- [9] Shizhao Xiong, Kai Xie, Erik Blomberg, Per Jacobsson, and Aleksandar Matic. Analysis of the solid electrolyte interphase formed with an ionic liquid electrolyte for lithium-sulfur batteries. *Journal of Power Sources*, 252:150 – 155, 2014.
- [10] K. Ghandi. A review of ionic liquids, their limits and applications. *Green and Sustainable Chemistry*, 4(1):44–53, 2014.
- [11] M. Montanino, S. Passerini, and G.B. Appetecchi. 4 - electrolytes for rechargeable lithium batteries. In Alejandro A. Franco, editor, *Rechargeable Lithium Batteries*, Woodhead Publishing Series in Energy, pages 73 – 116. Woodhead Publishing, 2015.
- [12] Ionic liquids. <http://www.sigmaaldrich.com/technical-documents/articles/chemfiles/ionic-liquids1.html>. Accessed: 2017-02-24.
- [13] Dr. G. W. H. Höhne, Dr. W. F. Hemminger, and Dr. H.-J. Flammersheim. *Differential Scanning Calorimetry*. Springer Berlin Heidelberg, second edition, 2003.

- [14] P. Gabbott. *A Practical Introduction to Differential Scanning Calorimetry, in Principles and Applications of Thermal Analysis* (ed P. Gabbott). Blackwell Publishing Ltd, Oxford, UK, 2008.
- [15] Thomas L. James. Chapter 1 - introduction. In Thomas L. James, editor, *Nuclear Magnetic Resonance in Biochemistry*, pages 1 – 14. Academic Press, 1975.
- [16] Georgy Salnikov Rainer Kerssebaum. *DOSY and Diffusion by NMR*. Bruker BioSpin GmbH, Reihnstetten, Germany, 2.0.0 edition, 2006.
- [17] Frédéric Leroy. Molecular driving forces. statistical thermodynamics in biology, chemistry, physics, and nanoscience. *Soft Materials*, 11(2):231–231, 2013.
- [18] N. Byrne, P. C. Howlett, D. R. MacFarlane, and M. Forsyth. The zwitterion effect in ionic liquids: Towards practical rechargeable lithium-metal batteries. *Advanced Materials*, 17(20):2497–2501, 2005.
- [19] Jianming Zheng, Meng Gu, Honghao Chen, Praveen Meduri, Mark H. Engelhard, Ji-Guang Zhang, Jun Liu, and Jie Xiao. Ionic liquid-enhanced solid state electrolyte interface (sei) for lithium-sulfur batteries. *J. Mater. Chem. A*, 1:8464–8470, 2013.
- [20] Qian Zhou, Wesley A. Henderson, Giovanni B. Appetecchi, Maria Montanino, and Stefano Passerini. Physical and electrochemical properties of n-alkyl-n-methylpyrrolidinium bis(fluorosulfonyl)imide ionic liquids: Py13fsi and py14fsi. *The Journal of Physical Chemistry B*, 112(43):13577–13580, 2008. PMID: 18828629.
- [21] Hyungook Yoon, Adam S. Best, Maria Forsyth, Douglas R. MacFarlane, and Patrick C. Howlett. Physical properties of high li-ion content n-propyl-n-methylpyrrolidinium bis(fluorosulfonyl)imide based ionic liquid electrolytes. *Phys. Chem. Chem. Phys.*, 17:4656–4663, 2015.
- [22] Junhua Huang and Anthony F. Hollenkamp. Thermal behavior of ionic liquids containing the fsi anion and the li+ cation. *The Journal of Physical Chemistry C*, 114(49):21840–21847, 2010.
- [23] Anna Martinelli, Aleksandar Matic, Per Jacobsson, Lars Börjesson, Alessandra Fericola, and Bruno Scrosati. Phase behavior and ionic conductivity in lithium bis(trifluoromethanesulfonyl)imide-doped ionic liquids of the pyrrolidinium cation and bis(trifluoromethanesulfonyl)imide anion. *The Journal of Physical Chemistry B*, 113(32):11247–11251, 2009. PMID: 19621942.
- [24] N Amini D R MacFarlane, P Meakin and M Forsyth. Structural studies of ambient temperature plastic crystal ion conductors. *Journal of Physics: Condensed Matter*, 13(36), 2001.
- [25] Masashi Ishikawa, Toshinori Sugimoto, Manabu Kikuta, Eriko Ishiko, and Michiyuki Kono. Pure ionic liquid electrolytes compatible with a graphitized carbon negative electrode in rechargeable lithium-ion batteries. *Journal of Power Sources*, 162(1):658 – 662, 2006.
- [26] Hajime Matsumoto, Hikari Sakaebe, Kuniaki Tatsumi, Manabu Kikuta, Eriko Ishiko, and Michiyuki Kono. Fast cycling of li/licoo2 cell with low-viscosity ionic liquids based on bis(fluorosulfonyl)imide [fsi]-. *Journal of Power Sources*, 160(2):1308 – 1313, 2006.

- [27] Physico-chemical properties. <http://en.solvionic.com/products/1-butyl-1-methylpyrrolidinium-bistrifluoromethanesulfonylimide-99>. 9. Accessed: 2017-05-23.
- [28] Andrzej Lewandowski and Agnieszka Świdorska Mocek. Ionic liquids as electrolytes for li-ion batteries—an overview of electrochemical studies. *Journal of Power Sources*, 194(2):601 – 609, 2009.

A

Appendix

A.1 Diffusion coefficients

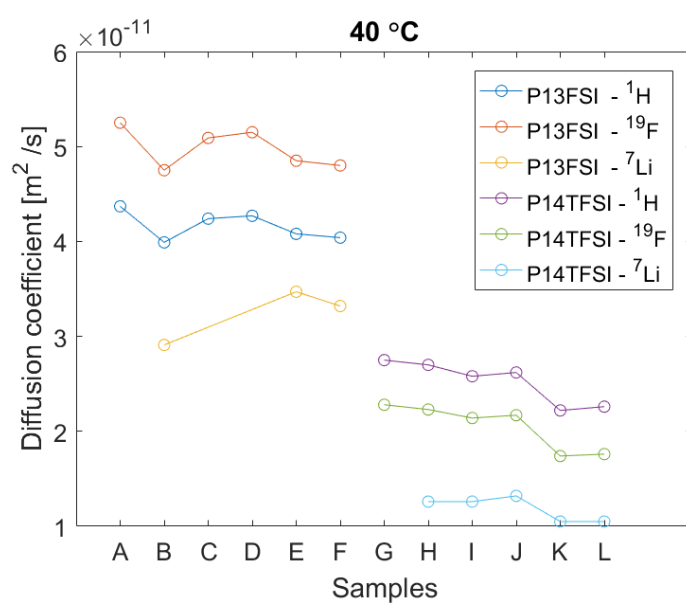


Figure A.1: Diffusion coefficients at 40 °C

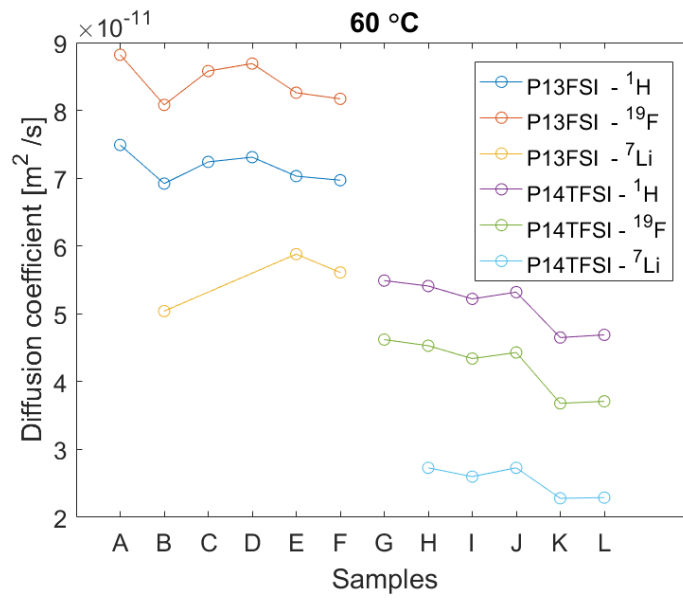


Figure A.2: Diffusion coefficients at 60 °C

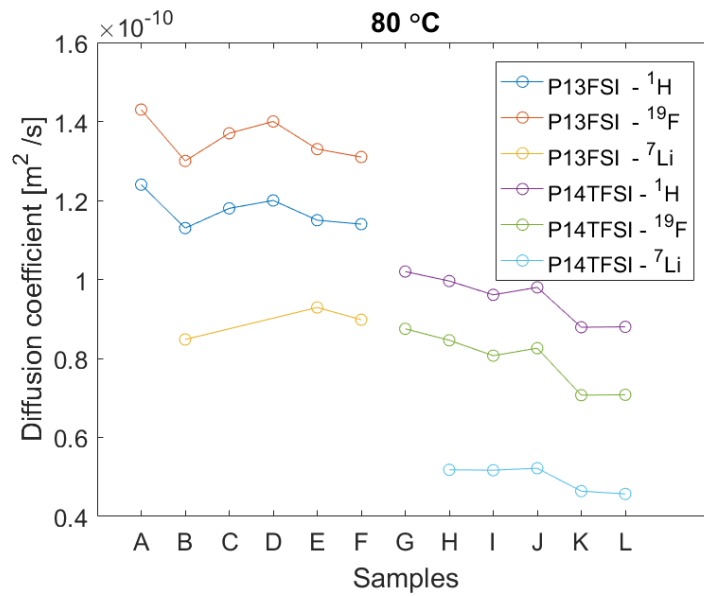


Figure A.3: Diffusion coefficients at 80 °C

A.2 Impedance

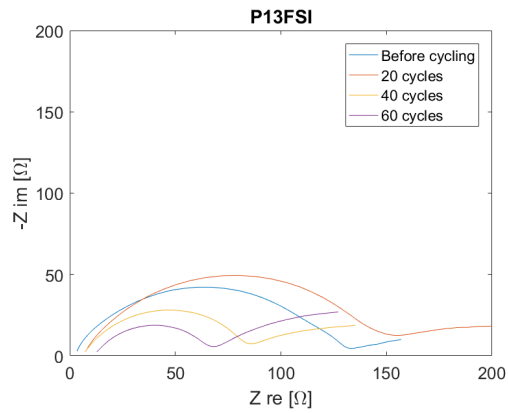


Figure A.4: Impedance spectrum of P13FSI

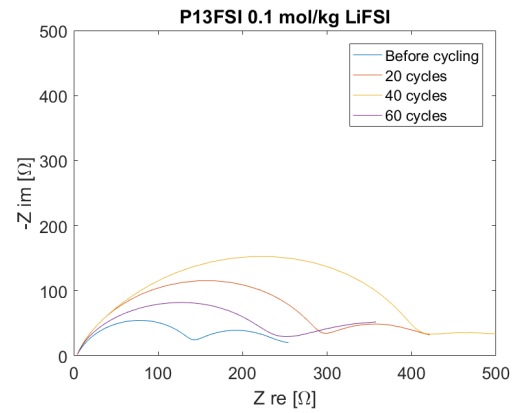


Figure A.5: Impedance spectrum of P13FSI 0.1 mol/kg LiFSI

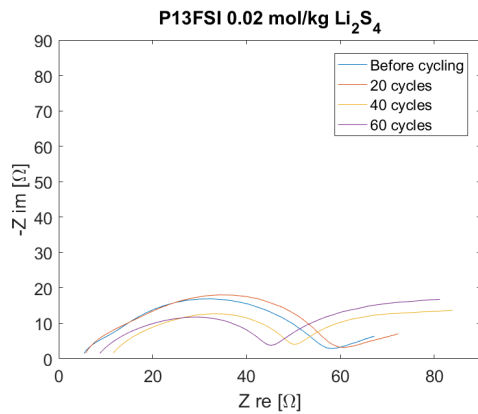


Figure A.6: Impedance spectrum of P13FSI 0.02 mol/kg Li_2S_4

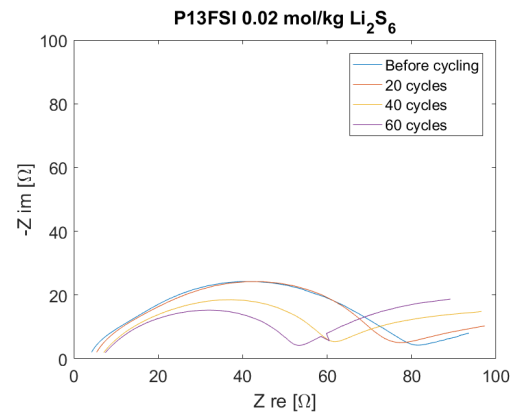


Figure A.7: Impedance spectrum of P13FSI 0.02 mol/kg Li_2S_6

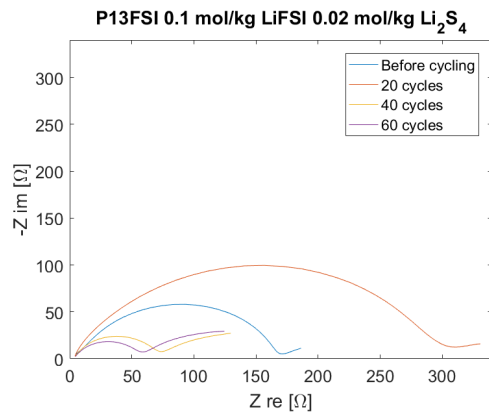


Figure A.8: Impedance spectrum of P13FSI 0.1 mol/kg LiFSI 0.02 mol/kg Li₂S₄

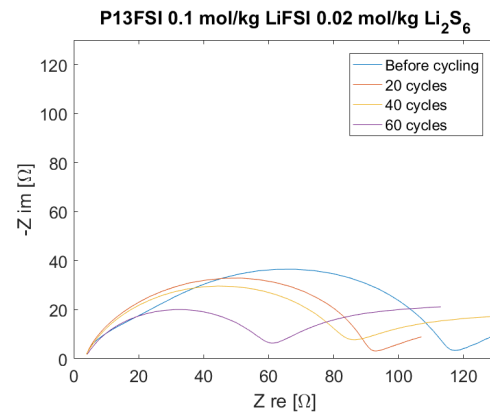


Figure A.9: Impedance spectrum of P13FSI 0.1 mol/kg LiFSI 0.02 mol/kg Li₂S₆

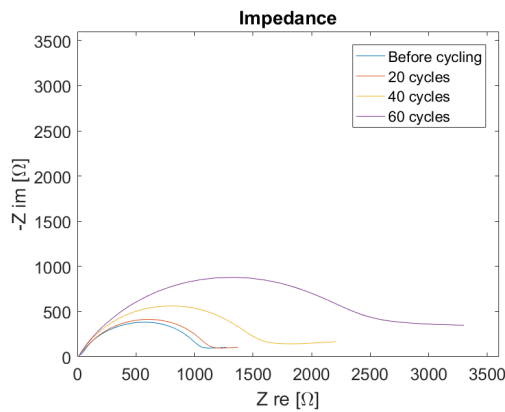


Figure A.10: Impedance spectrum of P14TFSI

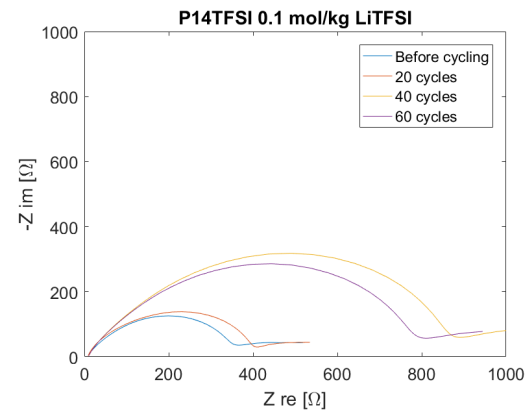


Figure A.11: Impedance spectrum of P14TFSI 0.1 mol/kg LiTFSI

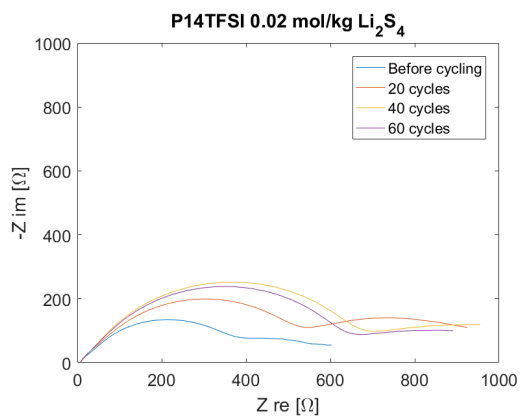


Figure A.12: Impedance spectrum of P14TFSI 0.02 mol/kg Li₂S₄

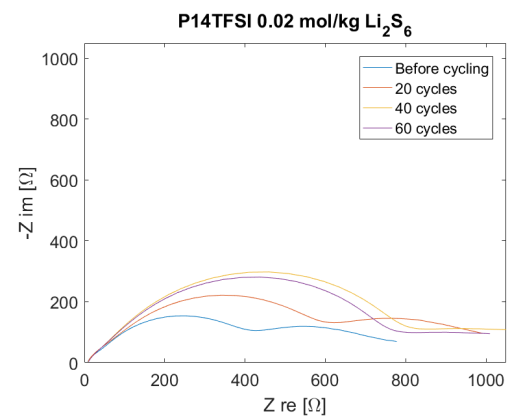


Figure A.13: Impedance spectrum of P14TFSI 0.02 mol/kg Li₂S₆

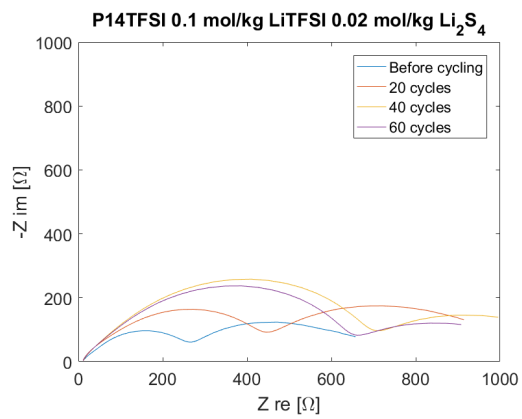


Figure A.14: Impedance spectrum of P14TFSI 0.1 mol/kg LiTFSI 0.02 mol/kg Li_2S_4

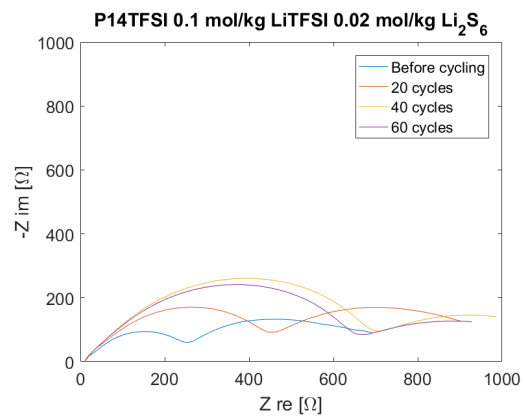


Figure A.15: Impedance spectrum of P14TFSI 0.1 mol/kg LiTFSI 0.02 mol/kg Li_2S_6

A.3 Cycling

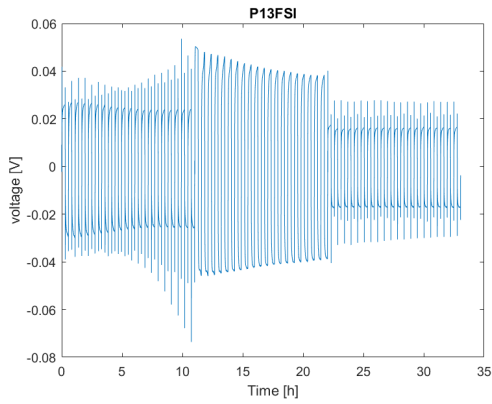


Figure A.16: Voltage profile for a symmetrical cell with a P13FSI electrolyte

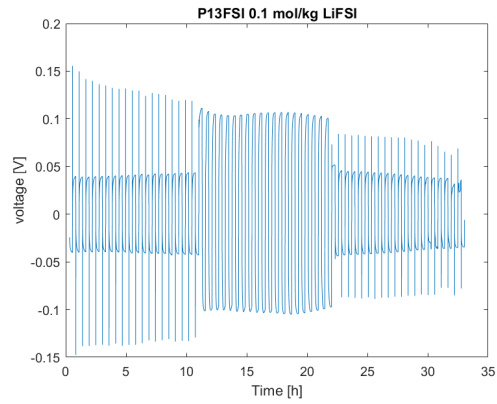


Figure A.17: Voltage profile for a symmetrical cell with a P13FSI 0.1 mol/kg LiFSI electrolyte

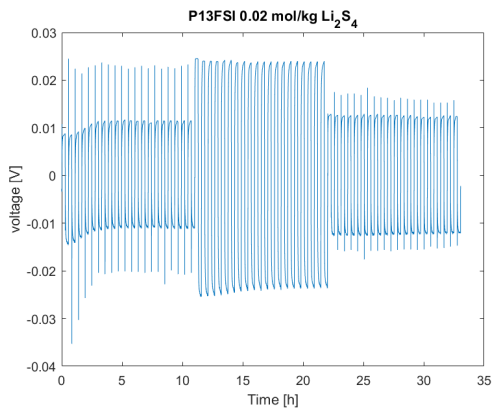


Figure A.18: Voltage profile for a symmetrical cell with a P13FSI 0.02 mol/kg Li_2S_4 electrolyte

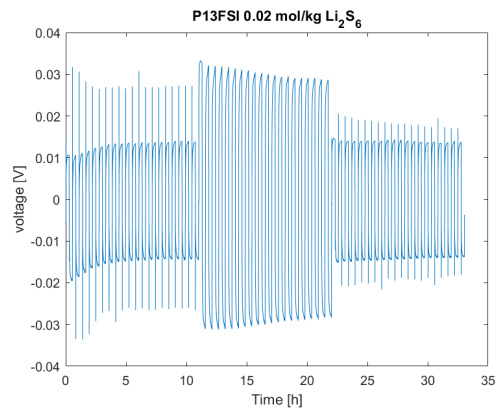


Figure A.19: Voltage profile for a symmetrical cell with a P13FSI 0.02 mol/kg Li_2S_6 electrolyte

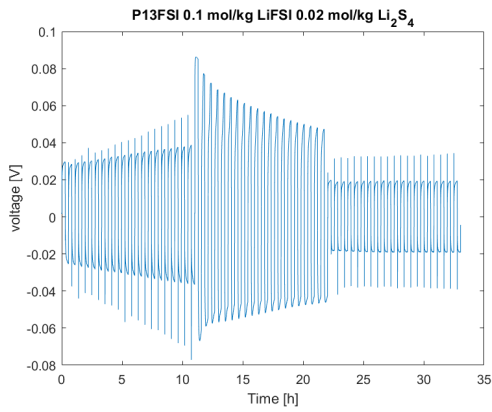


Figure A.20: Voltage profile for a symmetrical cell with a P13FSI 0.1 mol/kg LiFSI 0.02 mol/kg Li_2S_4 electrolyte

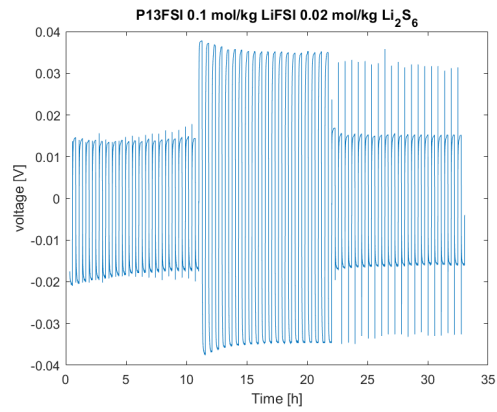


Figure A.21: Voltage profile for a symmetrical cell with a P13FSI 0.1 mol/kg LiFSI 0.02 mol/kg Li_2S_6 electrolyte

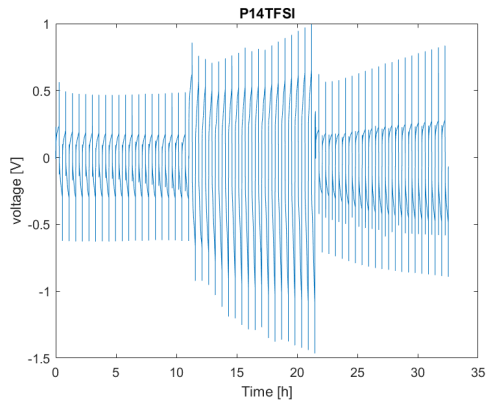


Figure A.22: Voltage profile for a symmetrical cell with a P14TFSI electrolyte

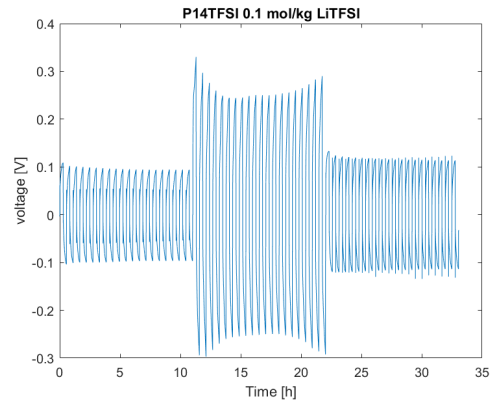


Figure A.23: Voltage profile for a symmetrical cell with a P14TFSI 0.1 mol/kg LiTFSI electrolyte

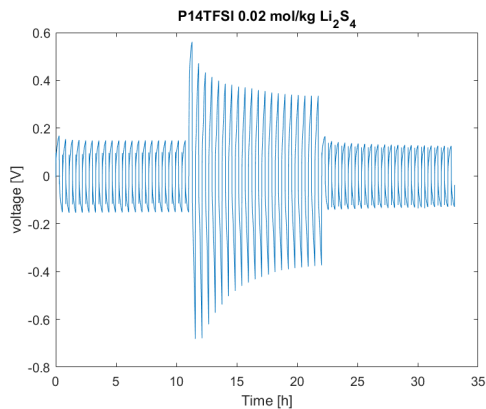


Figure A.24: Voltage profile for a symmetrical cell with a P14TFSI 0.02 mol/kg Li_2S_4 electrolyte

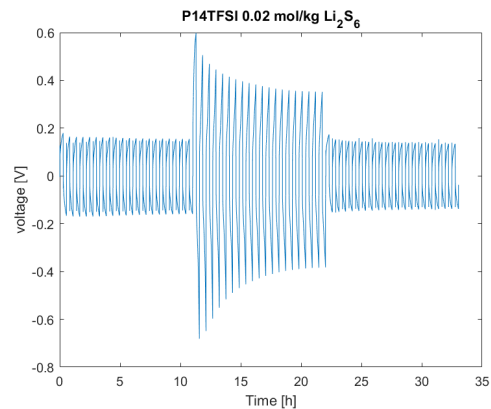


Figure A.25: Voltage profile for a symmetrical cell with a P14TFSI 0.02 mol/kg Li_2S_6 electrolyte

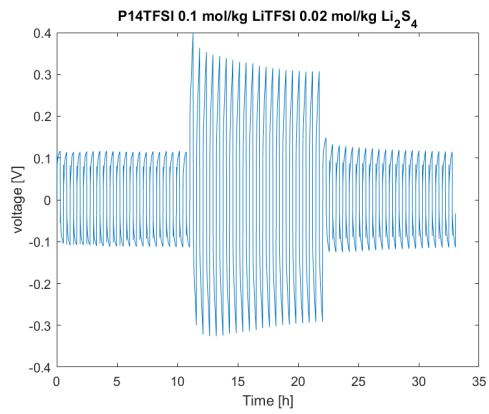


Figure A.26: Voltage profile for a symmetrical cell with a P14TFSI 0.1 mol/kg LiTFSI 0.02 mol/kg Li_2S_4 electrolyte

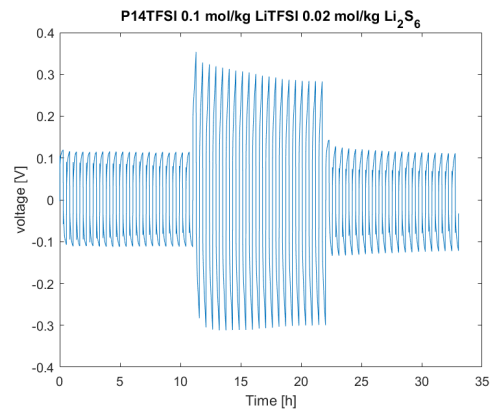


Figure A.27: Voltage profile for a symmetrical cell with a P14TFSI 0.1 mol/kg LiTFSI 0.02 mol/kg Li_2S_6 electrolyte